ACS Biomaterials SCIENCE & ENGINEERING

pubs.acs.org/journal/abseba

Article

The Impact of Tyrosine Iodination on the Aggregation and Cleavage Kinetics of MMP-9-Responsive Peptide Sequences

Douglas S. MacPherson, Scott A. McPhee, Brian M. Zeglis, and Rein V. Ulijn*

Cite This: *ACS Biomater. Sci. Eng.* 2022, 8, 579−587

Read Online

ACCESS | Metrics & More | Article Recommendations | Supporting Information

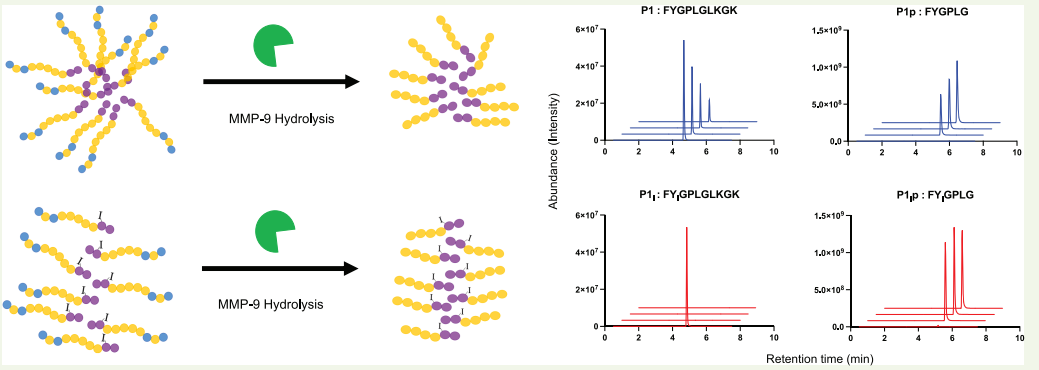

ABSTRACT: Matrix metalloproteinase (MMP) enzymes are over-expressed by some metastatic cancers, in which they are responsible for the degradation and remodeling of the extracellular matrix. In recent years, MMPs have emerged as promising targets for enzyme-responsive diagnostic probes because oligopeptides can be designed to be selectively hydrolyzed by exposure to these enzymes. With the ultimate goal of developing radio-iodinated peptides as supramolecular building blocks for MMP-sensitive tools for nuclear imaging and therapy, we designed three MMP-9-responsive peptides containing either tyrosine or iodotyrosine to assess the impact of iodotyrosine introduction to the peptide structure and cleavage kinetics. We found that the peptides containing iodotyrosine underwent more rapid and more complete hydrolysis by MMP-9. While the peptides under investigation were predominantly disordered, it was found that iodination increased the degree of aromatic residue-driven aggregation of the peptides. We determined that these iodination-related trends stem from the improved overall intramolecular order through H- and halogen bonding, in addition to intermolecular organization of the self-assembled peptides due to steric and electrostatic effects introduced by the halogenated tyrosine. These fundamental observations provide insights for the development of enzyme-triggered peptide aggregation tools for localized radioactive iodine-based tumor imaging.

KEYWORDS: *self-assembly, matrix metalloproteinases, enzyme-responsive materials, radio-iodine therapy, peptides, nanoscience, supramolecular organization*

1. INTRODUCTION

Matrix metalloproteinases (MMP) are enzymes that play vital roles in the growth and development of cells and tissues. MMPs are also over-expressed by some metastatic cancers, in which they are responsible for the degradation and remodeling of the extracellular matrix (ECM).[1] In light of this over-expression, MMPs have received attention as targets for enzyme-responsive diagnostic probes[2−5] and drug-delivery vectors.[6−9] It is now well established that ECM-derived peptide sequences containing 2−6 critical residues surrounding a hydrolyzable peptide bond can be selectively cleaved upon exposure to MMPs.[10,11] These sequences have been incorporated into the design of responsive nanoscale systems composed of inorganic nanoparticles[12,13] or peptide−polymer conjugates.[5,14−18] The combination of MMP-triggered peptide aggregation with nuclear probes containing a radioactive isotope of iodine would provide a means to target the activity of MMP-9 for imaging at the site of an MMP-expressing tumor. In this context, we are interested in studying the responsiveness of iodinated peptides designed to be preferentially hydrolyzed by MMP-9.

Based on previous reports on the effects of the incorporation of halogens on peptide self-assembly, we anticipated that the self-assembly of these peptides would be significantly impacted by the incorporation of iodine. The halogenation of self-

Received: November 23, 2021
Accepted: January 3, 2022
Published: January 20, 2022

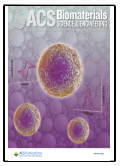

A.

Full Peptides			Hydrolysis Products		
Peptide	Sequence	Expected/Measured Mass (MH^{+1})	Peptide	Sequence	Expected/Measured Mass (MH^{+1})
P1	FYGPLGLKGK	1079.6248 / 1079.6241	**P1p**	FYGPLG	653.3293 / 653.3292
P2	KYFGPLGLKGK	1207.7198 / 1207.7209	**P2p**	KYFGPLG	781.4243 / 781.4232
P3	KKGPLGLAGFY	1150.6619 / 1150.6614	**P3p**	LAGFY	570.2922 / 570.2922
$P1_I$	$FY_IGPLGLKGK$	1205.5220 / 1205.5210	**$P1_Ip$**	FY_IGPLG	779.2265 / 779.2251
$P2_I$	$KY_IFGPLGLKGK$	1333.6170 / 1333.6162	**$P2_Ip$**	KY_IFGPLG	907.3215 / 907.3199
$P3_I$	$KKGPLGLAGFY_I$	1276.5591 / 1276.5574	**$P3_Ip$**	$LAGFY_I$	696.1894 / 696.1887

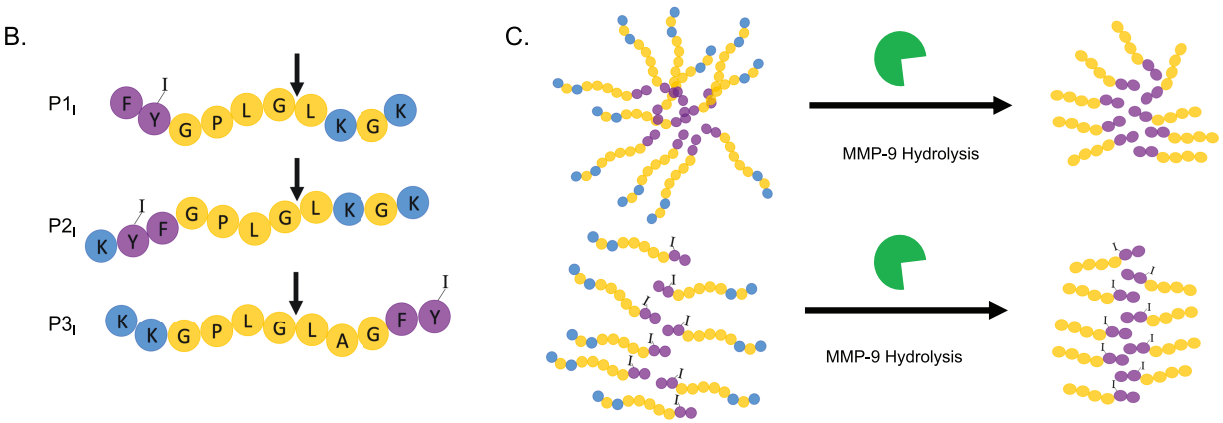

Figure 1. (A) Theoretical and experimentally determined monoisotopic mass for all peptides and expected hydrolysis products. (B) Representations of **$P1_I$**, **$P2_I$**, and **$P3_I$** indicating the functionally designed regions and sites of MMP-cleavage (arrows) and iodination (bracketed "I"). (C) Schematic of peptide self-assembly and hydrolysis into the tyrosine-bearing cleavage product by MMP-9 with an illustration of the differences in self-assembly upon peptide iodination.

assembling peptides has been shown to enhance the rate and degree of self-assembly as well as the rheological properties of the resulting supramolecular peptide network. In one example, the halogenation of self-assembling peptides has been shown to generate stiffer hydrogels that assemble more rapidly than analogous non-halogenated sequences.[20] Similarly, the introduction of an iodine to an amyloid-forming peptide sequence has been shown to lead to the formation of a strong hydrogel at lower concentrations compared to the halogen-free native peptide. The position of the iodine has also been shown to be influential, suggesting specific non-covalent interactions of the iodine atom in self-assembly.[21] The fluorination of self-assembling peptides influences their self-assembly behavior as well, producing distinctly different hierarchical arrangements in fluorinated versus non-fluorinated peptides.[22]

The MMP-mediated cleavage of self-assembling peptides has been used to induce morphological switching through the generation of fiber-forming peptide sequences following the hydrolysis of the parent peptide.[23,24] This approach has been combined with the encapsulation and release of drugs such as doxorubicin.[25] Similarly, the localized assembly of MMP-responsive co-polymers has been used to deliver an immunotherapeutic small molecule to a tumor site in a murine model.[6] Huang et al. recently demonstrated the MMP-9-triggered assembly of gold nanoparticles via electrostatic interactions following MMP-mediated dePEGylation. These nanoparticles underwent endocytosis and induced cytotoxicity in the MMP-9-expressing cells where inverting just two amino acids in this sequence inactivated the enzyme-responsiveness, self-assembly, and cellular uptake.[26] Enzyme-directed nanoparticle self-assembly at a tumor site was also used for in vivo cancer imaging based on kinetic trapping of the assembled particles within the tumor.[27] Another similar approach was predicated on the development of MMP-responsive, peptide-conjugated gold nanoclusters that took advantage of size-specific renal clearance. Upon exposure to MMP, the cleavage of the enzyme-sensitive peptides prompted the release of the nanoclusters, which were subsequently cleared and detected in urine based on their catalytic activity.[5]

A relationship between the efficiency of the hydrolysis of peptides by MMPs and the secondary structure of the self-assembled peptides has previously been observed. For example, changes in residues adjacent to the cleaved sequence of the MMP-responsive peptides have led to differences in hydrolysis rates despite the sequences having an identical core MMP-cleavable sequence.[28] In our previous work, we observed that the introduction of order-promoting (i.e., leucine, alanine) or order-disrupting (i.e., glycine, proline) residues dictates both the supramolecular order and cleavage kinetics. The most rapidly hydrolysable sequences were found to strike a balance between order and disorder, whereas the strongly self-assembled, amyloid-like systems as well as the unassembled structures both show poor degradation kinetics. In addition, the overall charge of supramolecular assemblies can strongly impact the interactions between the peptides and the enzyme through charge complementarity assisting in the interactions between enzymes and supramolecular substrates. Taking both factors into account, both the rate and extent of peptide cleavage can be controlled over several orders of magnitude, even for the sequences containing the same central MMP-cleavable peptide.[24]

Based on these previous observations, it is evident that the rate and extent of the hydrolysis of peptides by MMP-9 are expected to be significantly influenced by the introduction of

https://doi.org/10.1021/acsbiomaterials.1c01488
ACS Biomater. Sci. Eng. 2022, 8, 579−587

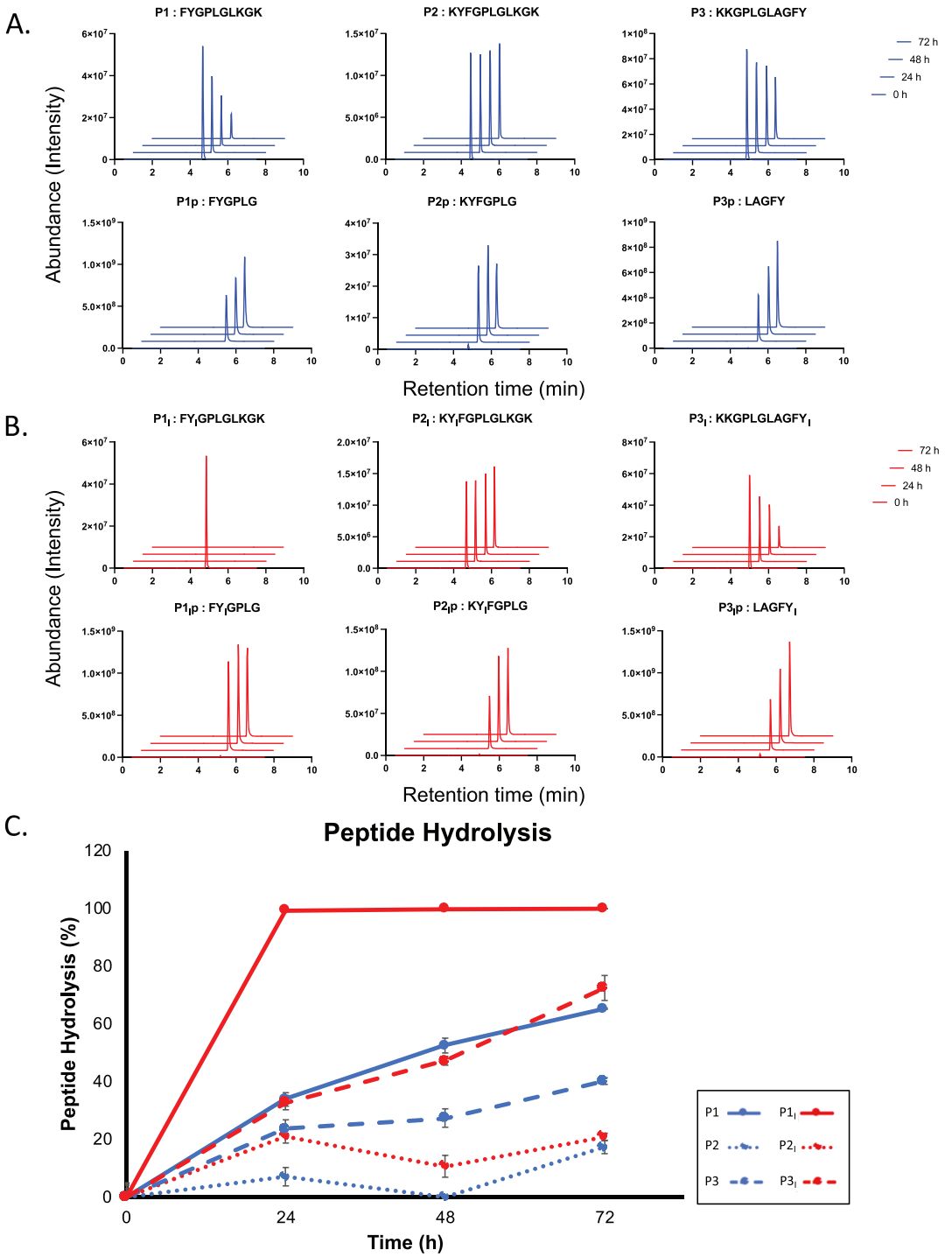

Figure 2. (A) The hydrolysis of **P1**, **P2**, and **P3** and the generation of the expected tyrosine-bearing cleavage products resulting from 72 h of reaction with MMP-9. (B) The hydrolysis of $\mathbf{P1_I}$, $\mathbf{P2_I}$, and $\mathbf{P3_I}$ and the generation of the expected iodotyrosine-bearing cleavage products resulting from 72 h of incubation with MMP-9. For both (A) and (B), LC−MS extracted ion chromatograms (EIC) were obtained from a reaction of 1.0 mM peptide and 100 ng/mL MMP-9. One of the three triplicates represented. (C) Peptide hydrolysis as a function of time for **P1**, $\mathbf{P1_I}$, **P2**, $\mathbf{P2_I}$, **P3**, and $\mathbf{P3_I}$.

iodo-tyrosine, either indirectly through differential aggregation—which impacts both the packing and enzyme access—or directly through a change in recognition and association by the enzyme due to the presence of a large electronegative atom (i.e., the iodine). Based on these previous reports, we set out to establish the impact of the incorporation of iodine on the behavior of a set of MMP-responsive peptide sequences.

2. RESULTS AND DISCUSSION

2.1. Peptide Sequence Design. A total of six (three tyrosine- and three iodotyrosine-containing), loosely aggregating peptide sequences are reported herein. In each case, we analyzed the same sequence containing either tyrosine or L-3-iodotyrosine. Future applications of our MMP-responsive peptide sequences will involve labeling the tyrosine within

https://doi.org/10.1021/acsbiomaterials.1c01488
ACS Biomater. Sci. Eng. 2022, 8, 579−587

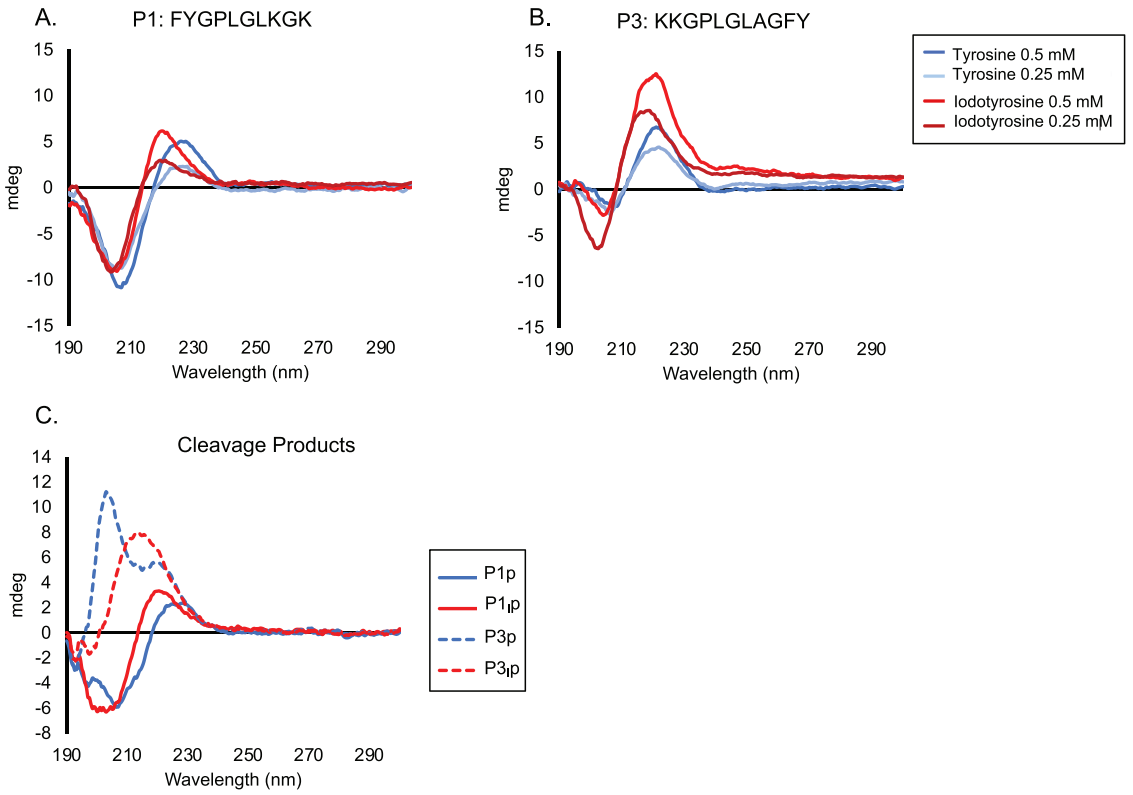

Figure 3. CD spectra of (A) **P1** and $\mathbf{P1_I}$ and (B) **P3** and $\mathbf{P3_I}$ comparing self-assembly between sequences containing tyrosine vs iodotyrosine at 0.25 and 0.5 mM. The peak shape and position are indicative of primarily random coil secondary structures with some β-turn characteristics. The addition of iodine results in slight blue-shifts for both sequences as well as changes in peak intensity for **P3**. (C) CD spectra of the expected tyrosine-bearing cleavage products—**P1p**, $\mathbf{P1_Ip}$, **P3p**, and $\mathbf{P3_Ip}$—comparing self-assembly between sequences containing tyrosine vs iodotyrosine at 0.25 mM. The addition of iodine results in a slight blue-shift in **P1** and a significant red shift as well as a loss of intensity in **P3**.

the peptide with radioactive—or "hot"—iodine, producing iodotyrosine (i.e., iodine-124 or iodine-131).[19] However, all experiments reported here used non-radioactive—or "cold"—iodine. In an aqueous environment, these peptides are designed to aggregate through both aromatic stacking and hydrophobicity.[29] We designed three MMP-9-responsive peptide sequences that we expected to guide our understanding of future iodine-bearing imaging agents. In brief, the rationale behind sequences 1, 2, and 3 (Figure 1) is as follows. Sequence 1 (**P1**) is an adaptation of a previous design—FFGPLGLKGK—which was demonstrated to undergo efficient cleavage,[24] with the cleavage product (FFGPLG) self-assembling into fibers because the FF dyad is a strong driver of self-assembly.[30] Yet here, we exchanged one F aromatic residue for Y, or Y_I. It is expected that this substitution with Y would reduce the self-assembly propensity of the sequence, whereas Y_I may enhance it based on the aforementioned previous research.[20−22] Sequence 2 (**P2**) is based on **P1** but with an added K on the *N*-terminus, giving us a terminal tripeptide KYF, which in isolation is a hydrogel-forming sequence with high self-assembly propensity.[31] Finally, for Sequence 3 (**P3**), we employed the MMP-9-cleavable sequence used in **P1** and **P2** with the approximately inversed aromatic and polar/charged regions at the *N*- and *C*-termini (Figure 1).

2.2. Peptide Hydrolysis by MMP-9 Measured by Quantitative LC−MS. Each of the peptides studied was fully soluble, and no macroscopic changes in the solution (e.g., precipitation, visible aggregation, or gelation) were observed when dissolved in PBS. When MMP-9 was added to the individual peptide solutions, we observed large differences in the hydrolysis rates of the iodinated and non-iodinated peptides as measured by quantitative liquid chromatography−mass spectrometry (LC−MS) analysis. The quantification of the peak areas of the peptides tracked the loss of the peptide as well as the enzymatic generation of the expected cleavage product over time (Figure 2A−C). **P1** showed the fastest initial rate and the greatest extent of hydrolysis and the greatest difference upon the incorporation of iodine, which resulted in a faster hydrolysis rate (i.e., 100% (±0.02%) hydrolysis by 24 h). Further investigation revealed that iodinated **P1**—($\mathbf{P1_I}$)—underwent complete hydrolysis (±0.06%) by 12 h (Supplementary Figure 1). In contrast, **P1** exhibited approximately 35% (±2.32%) hydrolysis after 24 h and 65% (±0.22%) after 72 h (Figure 2A−C). Neither the standard nor iodinated ($\mathbf{P2_I}$) **P2** displayed significant hydrolysis (Figure 2A−C). Finally, **P3** also demonstrated substantial hydrolysis although not to the extent of **P1**, with approximately 40% (±2.33%) hydrolysis of the non-iodinated peptide and 70% (±1.31%) hydrolysis of the iodinated peptide ($\mathbf{P3_I}$) by the 72 h endpoint (Figure 2A−C). For comparison, the sequence from which **P1** was derived—FFGPLGLKGK—underwent approximately 65% hydrolysis by 24 h and 100% hydrolysis by 48 h.[24] Generation of the expected tyrosine or iodotyrosine-bearing cleavage products was detectable for all sequences. In some cases, the relative abundance of the cleavage product was reduced in later timepoints due to the further digestion of the peptide fragments by MMP-9 (Figure 2A,B). While the expected cleavage product was dominant in the LC−MS chromatograms, the off-target cleavage was

https://doi.org/10.1021/acsbiomaterials.1c01488
ACS Biomater. Sci. Eng. 2022, 8, 579−587

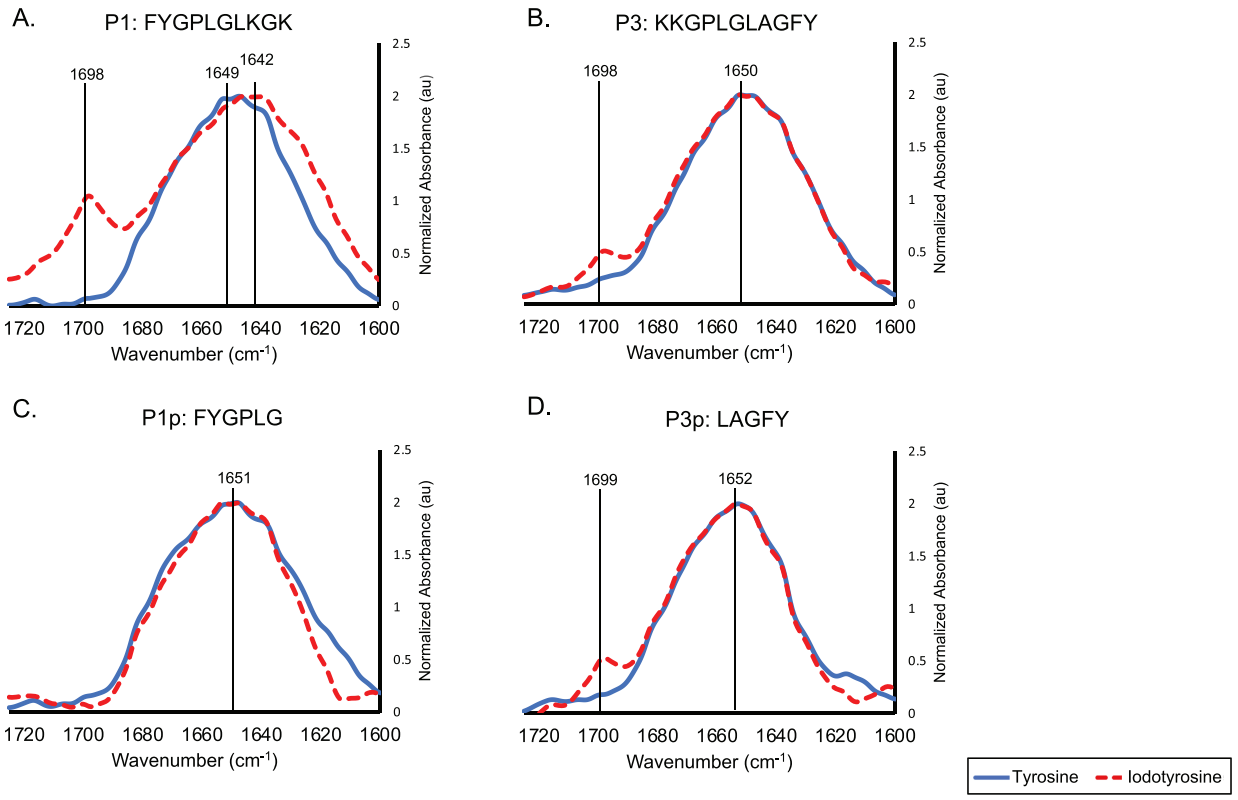

Figure 4. FTIR spectra of (A) **P1** and $\mathbf{P1_I}$, (B) **P3** and $\mathbf{P3_I}$, (C) **P1p** and $\mathbf{P1_Ip}$, and (D) **P3** and $\mathbf{P3_Ip}$ comparing the secondary structures of sequences containing tyrosine vs iodotyrosine at 20 mM. The spectra for both sequences are characteristic of a random coil (1650 cm^{-1}). The iodination of **P1** introduces β-turn (blue-shifted) and β-sheet (1700 cm^{-1}) signatures. The iodination of **P2** introduces beta-turn characteristic. The iodination of **P1p** produces no change. The iodination of **P3p** introduces a β-turn characteristic.

detectable. For example, for **P1**, the expected product is FYGPLG. A targeted screening approach for alternative hydrolysis products revealed the presence of the sequence FYGPL. Importantly, the two responsive sequences—**P1** and **P3**—share an FY dyad and a net charge of +2 on either of the peptide termini suggesting that Y_I introduction is permissible at both termini. In contrast, the unresponsive sequence—**P2**—does not share these design features with the charged residues present on both ends. Because **P2** was not hydrolyzed, it was omitted from further investigation.

2.3. Circular Dichroism Analysis of Peptide Self-Assembly. We theorized that the differences in the cleavage rates by MMP-9 between the iodinated and non-iodinated peptides, although only loosely aggregating in each case, could be attributed to differences in the folding, aggregation propensity, and packing of the peptides, thereby impacting the enzyme accessibility to the cleavable sites. This is expected to impact the accessibility of individual sequences by the enzyme, as observed previously when systematically modifying the peptide sequences.[24] To probe for the possible relationships between assembly and hydrolysis, we analyzed the structural features of **P1**, $\mathbf{P1_I}$, **P3**, and $\mathbf{P3_I}$ by circular dichroism (CD), Fourier-transform infrared spectroscopy (FTIR), and fluorescence spectroscopy.

We first performed CD spectroscopy on **P1**, $\mathbf{P1_I}$, **P3**, and $\mathbf{P3_I}$ in phosphate buffer at 0.25 and 0.5 mM to investigate the differences in the assembly of the sequences containing tyrosine vs iodotyrosine. One initial observation from CD is that the four peptides are all significantly disordered. The CD spectrum of **P1** shows a peak shape and position, which is characteristic of a random coil, with a possible β-turn component as indicated by a maximum absorbance at approximately 225 nm and a minimum at 205 nm,[32,33] confirming that these structures are loosely aggregating, with a β-turn tendency observed due to the Gly-Pro (GP) motif.[34] The spectrum of $\mathbf{P1_I}$ exhibits a similar peak shape but with a minor shift toward lower wavelengths, indicating less optimized aromatic stacking[35] (Figure 3A). This blue-shift is likely due to the bulkiness of the iodine atom creating steric hindrance between the aromatic groups of the self-assembling peptides and may also result from the changes in the aromatic interactions due to its electron-withdrawing nature.[20] While the intensity is higher for the 0.5 mM concentration, the spectra obtained at the two concentrations evaluated approximately overlay, and a slight blue-shift is observed for both. As expected for a soluble system, the higher concentration has a more intense signal of comparable shape. The CD spectrum of **P3** is similar in shape and position to that of **P1**, although with a comparatively reduced minimum, suggesting a random coil and β-turn. Upon iodination, self-assembly becomes more pronounced, with higher maxima and minima observed. Compared to **P1**, the peak shapes of **P3** and $\mathbf{P3_I}$ are more characteristic of β-turns. The peak position, however, is closer to that of a random-coil, with the spectra crossing the x-axis at approximately 210 nm.[32,33] The slight blue shift observed upon the iodination of **P1** is also observed in both concentrations of **P3** (Figure 3B). Similarly, a higher concentration of peptide produces a CD signal of higher intensity for **P3**. The above findings are consistent between the two concentrations assessed.

https://doi.org/10.1021/acsbiomaterials.1c01488
ACS Biomater. Sci. Eng. 2022, 8, 579−587

Taken together, these results indicate that while **P1** and **P3** are primarily disordered, MMP-9 preferentially hydrolyzes the peptides with less optimized aromatic stacking. Because FY is not as strong a driver of self-assembly as FF,[30,31] the FY mutation reduces the self-assembly propensity of the sequence, leading to a primarily disordered structure. CD spectroscopy of the synthesized cleavage products for **P1**—**P1p** and **P1$_I$p**—reveals a similar peak shape, position, and peak relationship compared to the full, intact peptides. For **P3**, however, **P3p** is blue-shifted compared to **P3$_I$p**, which is the opposite trend observed for all other sequences and concentrations. The spectrum of **P3p** also reaches a higher maximum compared to that of **P3$_I$p** at the same concentration, which is also the opposite of what was observed for **P3** (Figure 3C). **P3p** and **P3$_I$p** also have a peak shape resembling the β-sheet,[32,33] suggesting that this sequence holds promise for localized assembly post-MMP cleavage. The loss of polar residues between **P3** and **P3p** results in a change in the participating drivers of self-assembly. This would explain why sequence **P3p** has a different response to iodination compared to **P1**, **P3**, and **P1p**.

2.4. Secondary Structure Characterization by FTIR. We next employed FTIR to gain a better understanding of the changes in the H-bonding patterns and peptide secondary structure of **P1**, **P1$_I$**, **P3**, and **P3$_I$**. The samples were prepared at a concentration of 20 mM[24] in D_2O. The amide I band of **P1** shows a maximum at 1649 cm^{-1}, indicating the predominantly random coil structure and confirming the CD data. This is comparable to the original version of the sequence by Son et al. with an FF dyad rather than FY, which produced a maximum of 1642 cm^{-1} and exhibits a predominantly disordered structure.[24] The iodination of **P1** results in the generation of a second peak at approximately 1700 cm^{-1}, which is indicative of a β-turn contribution. Iodination also resulted in a slight shift of the original peak to 1642 cm^{-1}, which broadens the peak into the 1624−1640 cm^{-1} range that is characteristic of a β-sheet[36,37] (Figure 4A). Similar to **P1**, the amide I peak of **P3** has a maximum at 1650 cm^{-1}, suggesting a random coil structure. The iodination of **P3** did not result in any observable peak shifts. However, the introduction of the iodotyrosine did introduce a second peak, the same β-turn 1700 cm^{-1} peak observed in **P1$_I$** (Figure 4B). FTIR analysis indicates that both sequences—particularly **P1**—showed an increase in peptide organization upon the introduction of the iodotyrosine. Both sequences contain Gly-Pro motifs that are common contributors to the β-turn structure, in which hydrogen bonds are formed between backbone residues.[34] It is likely that the iodine introduces a halogen bond between residues,[38] increasing the inter- and intra-molecular order of the peptides and enhancing the β-turn propensity. These results suggest that MMP-9 preferentially hydrolyzes peptides that are arranged into more organized β-turn structures compared to the fully unstructured peptides. The evaluation of the synthesized cleavage products by FTIR shows the characteristic signature of random coil morphology for **P1p** and **P3p**. While still predominantly random coils, iodination generates a 1700 cm^{-1} β-turn peak for **P3$_I$p** but not for **P1$_I$p** (Figure 4C,D).

2.5. Fluorescence Analysis of Peptide Self-Assembly. Thus far, our observations indicate that iodination gives rise to a rebalancing of order and disorder, with a significant consequence for the rates of hydrolysis. To investigate this aspect further, we next sought to establish to what extent the tyrosine or iodotyrosine residues are exposed by observing any shifts in the native fluorescence of the tyrosine. These experiments were performed in PBS at 1.0, 0.5, 0.25, and 0.125 mM with an excitation wavelength of 270 nm. Compared to **P1**, **P3** showed approximately double the fluorescence intensity at the same concentrations. This observation suggests that **P1** has comparatively stronger inter-peptide aromatic-driven aggregation, effectively burying the tyrosine residue within the hydrophobic environment and reducing the intensity of emission. The iodinated versions show reduced fluorescence intensity[39] when compared at the same excitation wavelength. It is notable that the intensity observed for **P3$_I$** is much reduced compared to that of **P1$_I$** (Figure 5A,B). Comparing **P1** and **P3**, the fluorescence evaluation suggests that MMP-9 preferentially hydrolyzes the more self-assembled sequence. The analysis of the synthesized cleavage products showed similar differences in overall fluorescence intensity between **P1p** and **P3p** (Figure 5A,B) but a deviation from a linear relationship between the concentration and intensity for **P1$_I$p** and **P3$_I$p** at 0.5 mM concentration, suggesting that iodination has more impact on the self-assembly of the shorter, less polar sequences (Supplemental Figure 2).

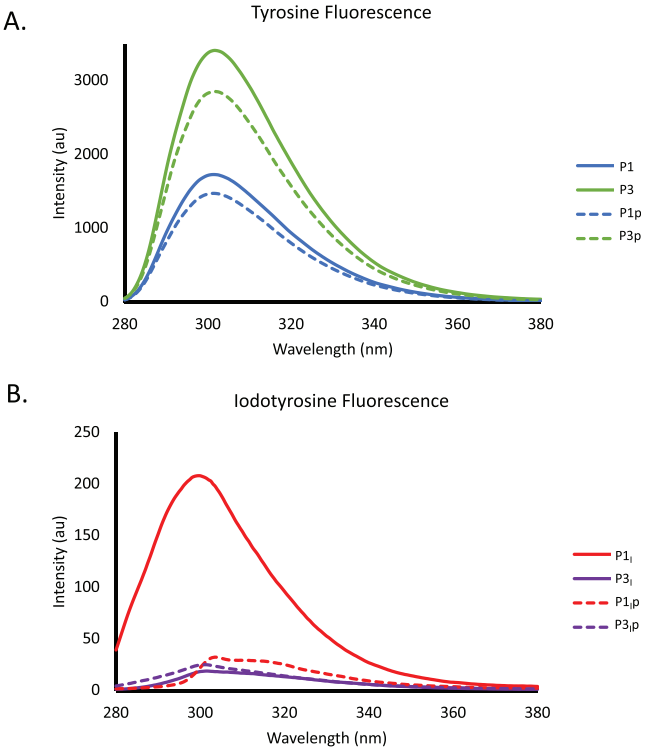

Figure 5. Fluorescence analysis of (A) **P1**, **P3**, **P1p**, and **P3p**; (B) **P1$_I$**, **P3$_I$**, **P1$_I$p**, and **P3$_I$p** comparing the overall intensity of tyrosine emission when excited at 270 nm. Peptides assessed at 1.0 mM. **P3** and **P3p** show higher overall fluorescence intensity than **P1** and **P1p**, indicating tighter aggregation of **P1** and **P1p**. All sequences show intensity reduction upon the addition of iodine, with **P1$_I$** showing the highest intensity compared to **P3$_I$**, **P1$_I$p**, and **P3$_I$p**.

3. DISCUSSION

The steric and electronic[20] effects introduced by iodotyrosine can likely alter the interactions between the peptide sequences and the binding site of the MMP-9 enzyme.[40] Charge and

https://doi.org/10.1021/acsbiomaterials.1c01488
ACS Biomater. Sci. Eng. 2022, 8, 579−587

polarity have an influence on the affinity of the enzyme for the peptide,[11,24,26,40,41] as illustrated by comparing **P1** and **P2**. **P1** undergoes rapid hydrolysis, whereas the addition of an *N*-terminal positively charged lysine (K) in **P2** completely inhibits hydrolysis. Likewise, **P3** contains the same MMP-cleavable sequence—GPLG—as **P1** as well as similar terminal amino acids: G, K and F, and Y. However, reversing the residues on the *N*- and *C*-termini in the sequence reduces the rate and extent of peptide hydrolysis between **P1** and **P3**. These findings can be understood in the context of the work by Huang et al., in which the addition of large aromatic substituents to the *N*-terminal of an MMP-cleavable peptide shifted the cleavage site toward the *N*-terminus and slowed down the hydrolytic rate. The researchers also found that longer peptides generally exhibited more efficient cleavage.[11] Overall, our data suggest that the introduction of 3-iodotyrosine in place of tyrosine increases the degree of intramolecular interactions by introducing halogen bonding to induce a structure within the individual peptides. The iodine also reduces intermolecular interactions by decreasing the degree of aromatic stacking between the peptides. We believe that both of these phenomena contribute to make the iodinated peptides better structured substrates that are also more accessible for MMP-9 and thus increase the hydrolytic activity.

4. CONCLUSIONS

We have demonstrated that iodinating the tyrosine of enzyme-responsive peptide sequences enhances hydrolysis by MMP-9, which is an unexpected and potentially beneficial feature for development of MMP-9 responsive radioiodine-based imaging probes. Our quantitative LC−MS analysis demonstrates that for the sequences assessed, MMP-9 cleaves between the G and L residues in the sequences with an FY dyad on one of the termini and a +2 net terminal charge. We believe that the faster cleavage of the iodinated peptides is a result of both the increased order of the peptide sequences and less optimized aromatic stacking, collectively leading to better accessibility of the individual peptides to the enzyme. Considering the physiological role of MMP-9 as a collagenase,[1] it is reasonable that the enzyme would preferentially hydrolyze a more organized structure.[42]

The electronic effects of the iodine also likely influence the interactions between the peptide and the enzyme. To translate our findings into clinically relevant designs, we initially predicted that the cleavage product of **P1** would self-assemble into fibers, as it is based on the sequence published by Son et al. in which the hydrolysis product—FFGPLG—assembled into fibers,[24] which we proposed could produce hydrophobic peptide nanofibers that accumulate in the vicinity of the MMP-9-secreting cancer cells.[24,25] Yet FF is a stronger driver of self-assembly than YF or FY,[31] and our data suggest loosely aggregated structures that do not form the intended fibers for the cleavage products (Supplementary Figure 3B). It is, however, possible that the inherent hydrophobicity of the sequence will confer some degree of adhesion to the tumor cells, anchoring the radioactive signal for imaging and therapy. The next steps will include the optimization of our sequence designs to form a more stable self-assembling structure, like the PhAc-FF cleavage product employed previously,[25] however retaining the required balance between order and disorder and taking advantage of the enhanced kinetics upon iodine introduction, to ensure that the time scales for activation are relevant for imaging applications. We will also explore a stronger, charge complementary self-assembling sequence that combines both the aromatic and electrostatic drivers of assembly, such as the sequence FEFK[43] (while replacing one F with Y to provide the site for iodination). In the end, we believe that the fundamental observation we have reported above—that the inclusion of iodotyrosines enhances the rate of MMP-mediated hydrolysis—provides useful insights into the development of clinically useful enzyme-responsive tools for nuclear imaging and therapy.

5. EXPERIMENTAL SECTION

5.1. Peptide Hydrolysis and Liquid Chromatography−Mass Spectrometry. All peptides were purchased from GenScript with a purity of >98% and TFA removed. The samples were dissolved at a concentration of 1.0 mM in 1× PBS supplemented with 1.0 mM $CaCl_2$ and 55 μM $ZnCl_2$ with the pH adjusted to 7.4. The catalytic domain (67 kDa) of the MMP-9 enzyme was produced by CalBiochem and purchased through Fischer Scientific (SKU #PF140, Batch #3534745). The enzyme was dissolved in 1× Tris-buffered saline (TBS) supplemented with the above $CaCl_2$ and $ZnCl_2$ concentrations and introduced to the peptide at a final concentration of 100 ng/mL. The reactions were stored at 37 °C, and triplicate samples of the reaction were taken at 0, 24, 48, and 72 h. The LC−MS samples were prepared with 20 μL of the reaction mixture added to 280 μL 1:1 ratio of MeCN:H_2O + 0.1% formic acid. Quantitative LC−MS was performed on a Thermo Fisher Exactive Plus LC−MS, with a gradient of MeCN:H_2O + 0.1% formic acid over 8 min through a Phenomenex luna omega 50 × 2.1 mm, 2.1 μm, 300A C18 column. Xcalibur processing software was used to identify the base peak of the peptide and to measure the peak area using the sum of charge states +1, +2, and +3 with caffeine as an internal standard.

5.2. Circular Dichroism of Self-Assembled Peptides. The peptide samples were prepared at concentrations of 0.25 and 0.5 mM for the full peptides and 0.25 mM for the synthesized cleavage products in 100 μM sodium phosphate buffer pH 7.4. Four hundred microliters of the sample was measured with a 0.1 cm path length quartz cuvette. The samples were measured on a Jasco J-1500 circular dichroism spectrophotometer at a range of 300−190 nm at a scanning speed of 100 nm/min.

5.3. Fourier Transform Infrared Spectroscopy of Peptides. The peptide samples were prepared at a concentration of 20 mM in D_2O. The sample solution was drop-cast between two CaF_2 cells with 12 μm PTFE spacers. The background was subtracted with a D_2O blank alone, the baseline was corrected, and the maximum intensities were normalized between the iodinated and non-iodinated sequences. The samples were measured on a Bruker Vertex 70 spectrometer with a nitrogen-flushed chamber. OPUS software was used to take measurements that were performed at a resolution of 4 cm^{-1}.

5.4. Fluorescence Intensity of Peptides. The peptide samples were prepared at a concentration of 1.0 mM in PBS at pH 7.4. The measurements were collected on a Jasco FP-8500 Spectrophotometer. The samples were excited at 270 nm, and the emission was collected from 280−380 nm at a scanning speed of 200 nm/min. Excitation and emission bandwidths were 5 and 2.5 nm, respectively.

■ ASSOCIATED CONTENT

Supporting Information

The Supporting Information is available free of charge at https://pubs.acs.org/doi/10.1021/acsbiomaterials.1c01488.

Peptide hydrolysis over 24 h (Figure S1); Fluorescence intensity analysis (Figure S2); Atomic force microscopy (Figure S3); Dynamic light scattering (Figure S4); Supplemental methods (PDF)

https://doi.org/10.1021/acsbiomaterials.1c01488
ACS Biomater. Sci. Eng. 2022, 8, 579−587

AUTHOR INFORMATION

Corresponding Author

Rein V. Ulijn − *Department of Chemistry, Hunter College of the City University of New York, New York, New York 10028, United States; Ph.D. Program in Biochemistry, The Graduate Center of the City University of New York, New York, New York 10016, United States; Advanced Science Research Center (ASRC) at The Graduate Center, City University of New York, New York, New York 10031, United States;* orcid.org/0000-0002-7138-1213; Email: RUlijn@gc.cuny.edu

Authors

Douglas S. MacPherson − *Department of Chemistry, Hunter College of the City University of New York, New York, New York 10028, United States; Ph.D. Program in Biochemistry, The Graduate Center of the City University of New York, New York, New York 10016, United States; Department of Radiology, Memorial Sloan Kettering Cancer Center, New York, New York 10065, United States; Advanced Science Research Center (ASRC) at The Graduate Center, City University of New York, New York, New York 10031, United States;* orcid.org/0000-0001-7973-3351

Scott A. McPhee − *Advanced Science Research Center (ASRC) at The Graduate Center, City University of New York, New York, New York 10031, United States*

Brian M. Zeglis − *Department of Chemistry, Hunter College of the City University of New York, New York, New York 10028, United States; Ph.D. Program in Biochemistry, The Graduate Center of the City University of New York, New York, New York 10016, United States; Department of Radiology, Memorial Sloan Kettering Cancer Center, New York, New York 10065, United States; Department of Radiology, Weill Cornell Medical College, New York, New York 10065, United States;* orcid.org/0000-0002-9091-744X

Complete contact information is available at: https://pubs.acs.org/10.1021/acsbiomaterials.1c01488

Author Contributions

R.V.U. and B.M.Z. raised conceptions and participated in the overall design, supervision, and coordination of the study. D.S.M. performed all of the experiments. S.A.M. helped to design the experiments and interpret the data. D.S.M, S.A.M, R.V.U., and B.M.Z. contributed to the writing, review, and revision of the manuscript. All authors read and approved the final manuscript.

Funding

This work is partially supported by the National Science Foundation CREST Center for Interface Design and Engineered Assembly of Low Dimensional systems (IDEALS), NSF grant number HRD-1547830, and Air Force Research Laboratory, grant number FA9550-19-1-0111.

Notes

The authors declare no competing financial interest.

ACKNOWLEDGMENTS

The authors would like to thank Dr. Ankit Jain of the CUNY Advanced Science Research center for his scientific advice in interpreting the CD data.

REFERENCES

(1) Gialeli, C.; Theocharis, A. D.; Karamanos, N. K. Roles of Matrix Metalloproteinases in Cancer Progression and Their Pharmacological Targeting: MMPs as Potential Targets in Malignancy. *FEBS J.* **2011**, *278*, 16−27.

(2) Olson, E. S.; Jiang, T.; Aguilera, T. A.; Nguyen, Q. T.; Ellies, L. G.; Scadeng, M.; Tsien, R. Y. Activatable Cell Penetrating Peptides Linked to Nanoparticles as Dual Probes for in Vivo Fluorescence and MR Imaging of Proteases. *Proceedings of the National Academy of Sciences* **2010**, *107*, 4311−4316.

(3) Stawarski, M.; Rutkowska-Wlodarczyk, I.; Zeug, A.; Bijata, M.; Madej, H.; Kaczmarek, L.; Wlodarczyk, J. Genetically Encoded FRET-Based Biosensor for Imaging MMP-9 Activity. *Biomaterials* **2014**, *35*, 1402−1410.

(4) Yi, D. K.; Sun, I.-C.; Ryu, J. H.; Koo, H.; Park, C. W.; Youn, I.-C.; Choi, K.; Kwon, I. C.; Kim, K.; Ahn, C.-H. Matrix Metalloproteinase Sensitive Gold Nanorod for Simultaneous Bioimaging and Photothermal Therapy of Cancer. *Bioconjugate Chem.* **2010**, *21*, 2173−2177.

(5) Loynachan, C. N.; Soleimany, A. P.; Dudani, J. S.; Lin, Y.; Najer, A.; Bekdemir, A.; Chen, Q.; Bhatia, S. N.; Stevens, M. M. Renal Clearable Catalytic Gold Nanoclusters for in Vivo Disease Monitoring. *Nat. Nanotechnol.* **2019**, *14*, 883−890.

(6) Battistella, C.; Callmann, C. E.; Thompson, M. P.; Yao, S.; Yeldandi, A. V.; Hayashi, T.; Carson, D. A.; Gianneschi, N. C. Delivery of Immunotherapeutic Nanoparticles to Tumors via Enzyme-Directed Assembly. *Adv. Healthcare Mater.* **2019**, *8*, 1901105.

(7) Ji, T.; Lang, J.; Wang, J.; Cai, R.; Zhang, Y.; Qi, F.; Zhang, L.; Zhao, X.; Wu, W.; Hao, J.; Qin, Z.; Zhao, Y.; Nie, G. Designing Liposomes To Suppress Extracellular Matrix Expression To Enhance Drug Penetration and Pancreatic Tumor Therapy. *ACS Nano* **2017**, *11*, 8668−8678.

(8) Kulkarni, P. S.; Haldar, M. K.; Nahire, R. R.; Katti, P.; Ambre, A. H.; Muhonen, W. W.; Shabb, J. B.; Padi, S. K. R.; Singh, R. K.; Borowicz, P. P.; Shrivastava, D. K.; Katti, K. S.; Reindl, K.; Guo, B.; Mallik, S. MMP-9 Responsive PEG Cleavable Nanovesicles for Efficient Delivery of Chemotherapeutics to Pancreatic Cancer. *Mol. Pharmaceutics* **2014**, *11*, 2390−2399.

(9) Chen, C.; Zhang, Y.; Hou, Z.; Cui, X.; Zhao, Y.; Xu, H. Rational Design of Short Peptide-Based Hydrogels with MMP-2 Responsiveness for Controlled Anticancer Peptide Delivery. *Biomacromolecules* **2017**, *18*, 3563−3571.

(10) West, J. L.; Hubbell, J. A. Polymeric Biomaterials with Degradation Sites for Proteases Involved in Cell Migration. *Macromolecules* **1999**, *32*, 241−244.

(11) Huang, Y.; Shi, J.; Yuan, D.; Zhou, N.; Xu, B. Length-Dependent Proteolytic Cleavage of Short Oligopeptides Catalyzed by Matrix Metalloprotease-9: Proteolytic Cleavage of Short Oligopeptides by MMPs. *Biopolymers* **2013**, *100*, 790−795.

(12) Gu, G.; Xia, H.; Hu, Q.; Liu, Z.; Jiang, M.; Kang, T.; Miao, D.; Tu, Y.; Pang, Z.; Song, Q.; Yao, L.; Chen, H.; Gao, X.; Chen, J. PEG-Co-PCL Nanoparticles Modified with MMP-2/9 Activatable Low Molecular Weight Protamine for Enhanced Targeted Glioblastoma Therapy. *Biomaterials* **2013**, *34*, 196−208.

(13) Nazli, C.; Demirer, G. S.; Yar, Y.; Acar, H. Y.; Kizilel, S. Targeted Delivery of Doxorubicin into Tumor Cells via MMP-Sensitive PEG Hydrogel-Coated Magnetic Iron Oxide Nanoparticles (MIONPs). *Colloids Surf., B* **2014**, *122*, 674−683.

(14) Zhu, L.; Perche, F.; Wang, T.; Torchilin, V. P. Matrix Metalloproteinase 2-Sensitive Multifunctional Polymeric Micelles for Tumor-Specific Co-Delivery of SiRNA and Hydrophobic Drugs. *Biomaterials* **2014**, *35*, 4213−4222.

(15) Ke, W.; Zha, Z.; Mukerabigwi, J. F.; Chen, W.; Wang, Y.; He, C.; Ge, Z. Matrix Metalloproteinase-Responsive Multifunctional Peptide-Linked Amphiphilic Block Copolymers for Intelligent Systemic Anticancer Drug Delivery. *Bioconjugate Chem.* **2017**, *28*, 2190−2198.

(16) Yao, Q.; Dai, Z.; Hoon Choi, J.; Kim, D.; Zhu, L. Building Stable MMP2-Responsive Multifunctional Polymeric Micelles by an

All-in-One Polymer−Lipid Conjugate for Tumor-Targeted Intracellular Drug Delivery. *ACS Appl. Mater. Interfaces* **2017**, *9*, 32520−32533.
(17) Peng, Z.-H.; Kopeček, J. Enhancing Accumulation and Penetration of HPMA Copolymer−Doxorubicin Conjugates in 2D and 3D Prostate Cancer Cells via IRGD Conjugation with an MMP-2 Cleavable Spacer. *J. Am. Chem. Soc.* **2015**, *137*, 6726−6729.
(18) Han, M.; Huang-Fu, M.-Y.; Guo, W.-W.; Guo, N.-N.; Chen, J.; Liu, H.-N.; Xie, Z.-Q.; Lin, M.-T.; Wei, Q.-C.; Gao, J.-Q. MMP-2-Sensitive HA End-Conjugated Poly(Amidoamine) Dendrimers via Click Reaction To Enhance Drug Penetration into Solid Tumor. *ACS Appl. Mater. Interfaces* **2017**, *9*, 42459−42470.
(19) Cao, J.; Wei, Y.; Zhang, Y.; Wang, G.; Ji, X.; Zhong, Z. Iodine-Rich Polymersomes Enable Versatile SPECT/CT Imaging and Potent Radioisotope Therapy for Tumor in Vivo. *ACS Appl. Mater. Interfaces* **2019**, *11*, 18953−18959.
(20) Ryan, D. M.; Anderson, S. B.; Nilsson, B. L. The Influence of Side-Chain Halogenation on the Self-Assembly and Hydrogelation of Fmoc-Phenylalanine Derivatives. *Soft Matter* **2010**, *6*, 3220.
(21) Bertolani, A.; Pirrie, L.; Stefan, L.; Houbenov, N.; Haataja, J. S.; Catalano, L.; Terraneo, G.; Giancane, G.; Valli, L.; Milani, R.; Ikkala, O.; Resnati, G.; Metrangolo, P. Supramolecular Amplification of Amyloid Self-Assembly by Iodination. *Nat. Commun.* **2015**, *6*, 7574.
(22) Sloand, J. N.; Culp, T. E.; Wonderling, N. M.; Gomez, E. D.; Medina, S. H. Mechanomorphogenic Films Formed via Interfacial Assembly of Fluorinated Amino Acids. *Adv. Funct. Mater.* **2021**, *31*, 2104223.
(23) Yang, Z.; Ma, M.; Xu, B. Using Matrix Metalloprotease-9 (MMP-9) to Trigger Supramolecular Hydrogelation. *Soft Matter* **2009**, *5*, 2546−2548.
(24) Son, J.; Kalafatovic, D.; Kumar, M.; Yoo, B.; Cornejo, M. A.; Contel, M.; Ulijn, R. V. Customizing Morphology, Size, and Response Kinetics of Matrix Metalloproteinase-Responsive Nanostructures by Systematic Peptide Design. *ACS Nano* **2019**, 1555.
(25) Kalafatovic, D.; Nobis, M.; Javid, N.; Frederix, P. W. J. M.; Anderson, K. I.; Saunders, B. R.; Ulijn, R. V. MMP-9 Triggered Micelle-to-Fibre Transitions for Slow Release of Doxorubicin. *Biomater. Sci.* **2015**, *3*, 246−249.
(26) Huang, R. H.; Nayeem, N.; He, Y.; Morales, J.; Graham, D.; Klajn, R.; Contel, M.; O'Brien, S.; Ulijn, R. V. Self-Complementary Zwitterionic Peptides Direct Nanoparticle Assembly and Enable Enzymatic Selection of Endocytic Pathways. *Adv. Mater.* **2022**, *34*, 2104962.
(27) Chien, M.-P.; Carlini, A. S.; Hu, D.; Barback, C. V.; Rush, A. M.; Hall, D. J.; Orr, G.; Gianneschi, N. C. Enzyme-Directed Assembly of Nanoparticles in Tumors Monitored by *in Vivo* Whole Animal Imaging and *Ex Vivo* Super-Resolution Fluorescence Imaging. *J. Am. Chem. Soc.* **2013**, *135*, 18710−18713.
(28) Shi, Y.; Ferreira, D. S.; Banerjee, J.; Pickford, A. R.; Azevedo, H. S. Tuning the Matrix Metalloproteinase-1 Degradability of Peptide Amphiphile Nanofibers through Supramolecular Engineering. *Biomater. Sci.* **2019**, *7*, 5132−5142.
(29) Fleming, S.; Ulijn, R. V. Design of Nanostructures Based on Aromatic Peptide Amphiphiles. *Chem. Soc. Rev.* **2014**, *43*, 8150−8177.
(30) Reches, M.; Gazit, E. Casting Metal Nanowires Within Discrete Self-Assembled Peptide Nanotubes. *Science* **2003**, *300*, 625−627.
(31) Frederix, P. W. J. M.; Scott, G. G.; Abul-Haija, Y. M.; Kalafatovic, D.; Pappas, C. G.; Javid, N.; Hunt, N. T.; Ulijn, R. V.; Tuttle, T. Exploring the Sequence Space for (Tri-)Peptide Self-Assembly to Design and Discover New Hydrogels. *Nature Chem* **2015**, *7*, 30−37.
(32) Brahms, S.; Brahms, J.; Spach, G.; Brack, A. Identification of , −Turns and Unordered Conformations in Polypeptide Chains by Vacuum Ultraviolet Circular Dichroism. *Proc. Natl. Acad. Sci.* **1977**, *74*, 3208−3212.
(33) Greenfield, N. J. Using Circular Dichroism Spectra to Estimate Protein Secondary Structure. *Nat. Protoc.* **2006**, *1*, 2876−2890.
(34) Hutchinson, E. G.; Thornton, J. M. A Revised Set of Potentials for β-Turn Formation in Proteins. *Protein Sci.* **1994**, *3*, 2207−2216.
(35) Pappas, C. G.; Abul-Haija, Y. M.; Flack, A.; Frederix, P. W. J. M.; Ulijn, R. V. Tuneable Fmoc−Phe−(4-X)−Phe−NH2 Nanostructures by Variable Electronic Substitution. *Chem. Commun.* **2014**, *50*, 10630−10633.
(36) Arunkumar, R.; Drummond, C. J.; Greaves, T. L. FTIR Spectroscopic Study of the Secondary Structure of Globular Proteins in Aqueous Protic Ionic Liquids. *Front. Chem.* **2019**, *7*, 74.
(37) Cobb, J. S.; Zai-Rose, V.; Correia, J. J.; Janorkar, A. V. FT-IR Spectroscopic Analysis of the Secondary Structures Present during the Desiccation Induced Aggregation of Elastin-Like Polypeptide on Silica. *ACS Omega* **2020**, *5*, 8403−8413.
(38) Robertson, C. C.; Wright, J. S.; Carrington, E. J.; Perutz, R. N.; Hunter, C. A.; Brammer, L. Hydrogen Bonding vs. Halogen Bonding: The Solvent Decides. *Chem. Sci.* **2017**, *8*, 5392−5398.
(39) Cowgill, R. W. Fluorescence and the Structure of Proteins IV. Iodinated Tyrosyl Residues. *Biochim. Biophys. Acta, Biophys. Incl. Photosynth.* **1965**, *94*, 74−80.
(40) Samarajeewa, S.; Zentay, R. P.; Jhurry, N. D.; Li, A.; Seetho, K.; Zou, J.; Wooley, K. L. Programmed Hydrolysis of Nanoassemblies by Electrostatic Interaction-Mediated Enzymatic-Degradation. *Chem. Commun.* **2014**, *50*, 968−970.
(41) Wang, M.; Zhang, Q.; Jian, H.; Liu, S.; Li, J.; Wang, A.; Dong, Q.; Ren, P.; Li, X.; Bai, S. Role of Thermolysin in Catalytic-Controlled Self-Assembly of Fmoc-Dipeptides. *CCS Chem.* **2020**, *2*, 317−328.
(42) Shoulders, M. D.; Raines, R. T. Collagen Structure and Stability. *Annu. Rev. Biochem.* **2009**, *78*, 929−958.
(43) Guilbaud, J.-B.; Vey, E.; Boothroyd, S.; Smith, A. M.; Ulijn, R. V.; Saiani, A.; Miller, A. F. Enzymatic Catalyzed Synthesis and Triggered Gelation of Ionic Peptides. *Langmuir* **2010**, *26*, 11297−11303.

https://doi.org/10.1021/acsbiomaterials.1c01488
ACS Biomater. Sci. Eng. 2022, 8, 579−587